Geophysical Modelling of a Sedimentary Portion of the White Volta Basin (Ghana)

Giulio Vignoli[1,2(✉)], Elikplim Abla Dzikunoo[3], Flemming Jørgensen[4], Sandow Mark Yidana[3], Bruce Banoeng-Yakubo[3], and Peng Bai[1]

[1] University of Cagliari, Cagliari, Italy
gvignoli@unica.it
[2] GEUS, Aarhus, Denmark
[3] University of Ghana, Accra, Ghana
[4] Central Denmark Region, Viborg, Denmark

Abstract. This research deals with the essential steps carried out during the processing and inversion of the airborne time-domain electromagnetic (TEM) data used within the framework of the GhanAqua project – aiming at the groundwater development for sustainable agriculture in the White Volta basin in Ghana.

The processing of pre-existing airborne TEM data has been performed with the state-of-the-art methodologies. In this respect, (1) the minimum possible gate-dependent lateral stacking between adjacent soundings has been performed for the preparation of the data; (2) a 1D nonlinear forward modelling has been used for the inversion of the stacked data; (3) even if the forward modelling was 1D, the data have been inverted by spatially constraining the adjacent models (in a pseudo-2/3D fashion). We adopted an iterative approach in which the processing and inversion parameters, and the type of stabilizer utilized, have been decided after an a-posteriori analysis. Hence, after every inversion, the results have been discussed with the geologists (1) to assess, at least qualitatively, the uncertainty of the solution features and (2) to, as much as possible, include prior geological knowledge into the geophysical analysis.

The new geophysical insights detected geological features that might be interpreted as glacial paleovalleys. If confirmed, those structures can have a significant impact in terms of their socio-economic relevance (i.e. as groundwater reservoirs); as well as from a scientific point of view (as they would require rethinking the stratigraphy of the area). In addition, these kind of Sturtian glacial evidences in West Africa could support the Snowball Earth hypothesis.

Keywords: Airborne transient electromagnetics · Sparse regularization · Conductivity depth image · Snowball earth · Paleovalleys

1 The Area and the Data

The investigated area is a sedimentary part of the White Volta basin (Fig. 1), with special focus on the project area: the Nasia Catchment – located in the north-eastern part of Ghana, between latitudes 9°55'N and 10°40'N, and longitude 1°05'W and 0°15'E.

© Springer Nature Switzerland AG 2020
O. Gervasi et al. (Eds.): ICCSA 2020, LNCS 12255, pp. 891–902, 2020.
https://doi.org/10.1007/978-3-030-58820-5_64

Large portions of Ghana have been studied by using several airborne geophysical methodologies during the European Union sponsored, Mining Sector Support Programme, from 2005 to 2010. These data include three regional surveys performed by Fugro Airborne Surveys and consisting of: a magnetic and gamma-ray spectrometry survey (line-spacing 500 m, alt. 120 m); a gravity survey (line-spacing 5000 m, alt.

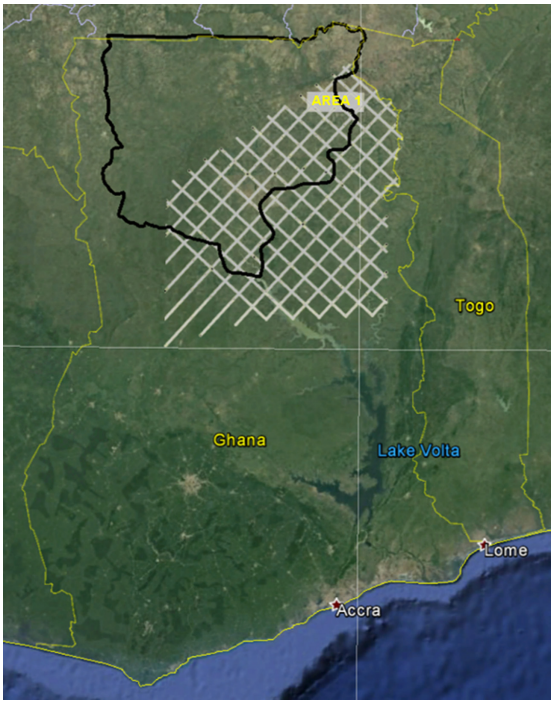

Fig. 1. Map of Ghana with the White Volta basin (within the black frame) together with the flight lines considered in the present research.

860 m); and a magnetic and TEM survey (line-spacing 20000 m). In addition, several higher resolution TEM surveys were performed, in which the line-spacing was significantly smaller (200 m). In Fig. 1, the flight-lines from the TEM surveys that have been considered in the present study are shown in grey. Hence, in this research, by the kind concession of the Ghana Geological Survey Authority (GGSA), and within the framework of the Memorandum of Understanding, signed on 23/03/2015 between the University of Ghana (UoG) and GGSA, we had the chance to work on part of the available regional dataset and on the high-resolution measurements collected over an area (Area 1) partially overlapping the Nasia catchment (Fig. 1). The airborne TEM data were collected by using a GEOTEM 20-channel multicoil system, with a transmitter area of 231 m^2 and 6 turns, at a nominal height of 120 m. The receiver was $\sim$130 m behind the center of the transmitting loop. The pulse width was 4066 μs, and the off-time 15834 μs. The nominal transmitter current was 560 A. During the

surveys all three components (X, Y, Z) were recorded. More details about the specifications of the data collection can be found in [1, 2].

The contractor supplied the raw data together with the associated Conductivity Depth Images [3]. Conductivity Depth Imaging (CDI) is a very effective tool for the detection of potential mineral targets. In fact, CDI provides a direct and fast translation of the measured data into electrical resistivity parameters with very high lateral resolution and with no need for a proper inversion or complex forward modelling of the underlying physical system [4]. However, since the GhanAqua project aims at the reconstruction of the geology and, in turn, of the hydrogeology, of the area, it was crucial to verify alternative approaches capable of retrieving relatively small resistivity variations while preserving the spatial coherence of the subsurface features. Thus, it has been necessary to verify the performances of an actual inversion of the data via a 1D nonlinear forward modelling code, spatially constraining the adjacent 1D resistivity models.

The raw data supplied by the contractor as the final deliverable were B-field data; besides the benefits discussed in [5], the choice of B-field has some additional advantages in terms of signal-to-noise ratio; in fact, the B-field is associated with data integration over time, that corresponds to some sort of data stacking in time. Moreover, to have a fair comparison between the CDIs and the inversion results (in order to properly assess what can be gained by a geomodelling-oriented processing and inversion), the original B-field data (and not the dB/dt measurements) have been reprocessed and utilized.

1.1 The First Processing Step: Lateral Stacking

Clearly, the data stacking can (should) be performed, not only in time (by considering the B-field measurements), but also in the other "direction", that is, spatially, along the line of flight. In the workflow implemented in this research, a moving window with a varying width depending on the considered time-gate has been used in a fashion similar to the one detailed, for example, in [10, 11] (in the latter, the stacking width is frequency-dependent). Hence, we used (i) a narrower stacking width for the early gates and (ii) a wider one for late gates. This allowed a maximization of the lateral resolution at shallow layers (early gates), and an increase of the robustness of the signal at depth (late gates) where, in any case, a larger spatial footprint is due to the physics of the method. In practice, the size of the window for the Z-component of the B-field was chosen to increase linearly from around 8 s, for the first gate (4.5 ms), to approximately 20 s, for the 11th gate (11.563 ms), and to remain constant for the last four gates. Only the Z and X components have been processed (using the same settings). Out of the 20 measured channels, after the lateral stacking, 15 channels have been used for the Z-component, and 12 for the X-component. The large number of channels that could be used demonstrate once again the very good quality of the data collected in the first place by Fugro. A sample of processed measurements is shown in Fig. 2.

The source waveform is quite stable in shape, whereas the same is not always true for the amplitude (Fig. 3). Even within the same flight, variations significantly larger than 10 A may occur, and they can be much larger if different flights are considered (while the nominal current is 560 A, the actual current peak can vary from 539 to 566 A

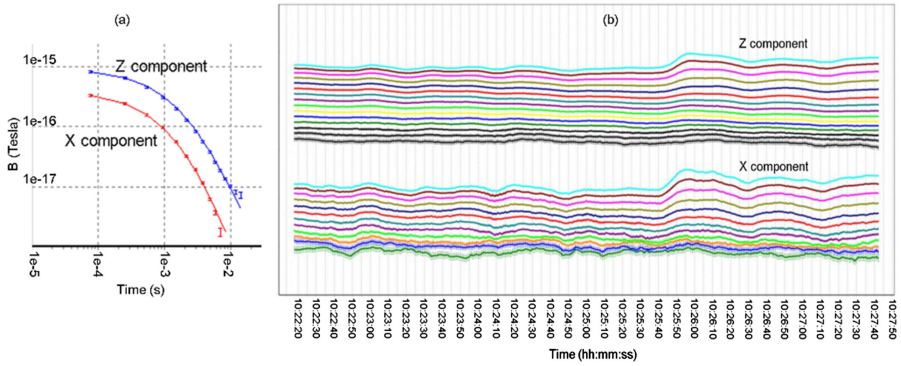

Fig. 2. (a) Example of the Z- and X-component records; the vertical bars represent the stacked data with their uncertainty; the solid lines show the calculated responses from the inversion model (not shown). (b) A sample of the B-field measurements obtained after the application of the spatial stacking procedure (moving window with gate-dependent width).

from flight to flight.). In any case, this variability has been properly taken into account during the inversion.

2 The Inversion

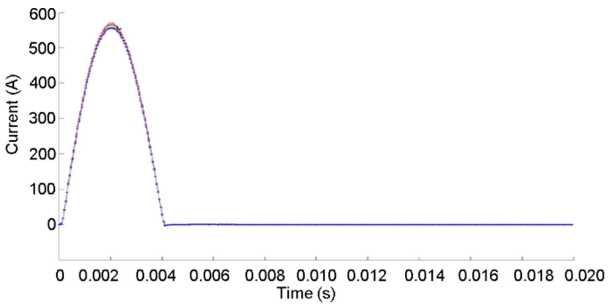

Fig. 3. Example of waveforms for the flight 71 in the Area 1.

Currently, 1D forward modelling algorithms which incorporate all the characteristics of the instrument's transfer function are efficient and popular choices [6]. However, 2D forward modelling codes [7], and even 3D [8] approaches, are becoming more and more frequently used. In this respect, there are many examples in literature which discuss the advantages of inversion schemes based on 1D or 2–3D forward modelling (e.g. [9, 12, 13]). The choice of a specific forward modelling is largely determined by the computational resources available. In fact, even with 1D algorithms, days, or even

weeks, might be necessary to invert large airborne datasets. Thus, for practical reasons, here, a 1D inversion approach has been used.

The inversion scheme employed includes different kinds of regularization to cope with the inherent ill-posedness of the problem. Testing different inversion approaches (each incorporating different prior information) allowed the implementation of an iterative geological-geophysical strategy for the inclusion of the geological knowledge into the inversion process and, to some extent, for the qualitative estimation of the uncertainty (Fig. 4). Even if the forward modelling used is 1D, the adjacent resistivity models were mutually constrained. In this way, it was possible to ensure some degree of lateral coherence between the neighboring 1D models and, also, within each individual 1D model. Thus, the regularization acted in both vertical and horizontal directions. The lateral and vertical constraints have been defined via the regularization term in the objective function minimized during the inversion. Several inversions were performed by using (i) minimum gradient support (MGS), (ii) L1-norm (MGN-L1), and (iii) minimum gradient L2-norm (MGN) regularizations, with different weights for the stabilizer.

So, the considered objective function $P_s(d_{obs}, m, \alpha)$ consists of the sum of the data misfit term, $\phi(d_{obs})$, and the stabilizer, $s(m)$ – with m being the resistivity model to be reconstructed and d_{obs} the observed data:

$$P_s(d_{obs}, m, \alpha) = \phi(d_{obs}) + \alpha s(m); \tag{1}$$

the factor α controls the importance/weight of the prior information (i.e. $s(m)$) with respect to the data. The data misfit $\phi(d_{obs})$ has been chosen equal to the $\frac{1}{N}\sqrt{\sum_{i=1}^{N}\left(\frac{d_{obs}-d_{calc}}{\sigma_d}\right)_i^2}$, in which: σ_d is an estimation of the uncertainty in the measurement, d_{calc} is the response calculated from m, and N is the number of measurements. α is chosen a-posteriori in order to get $\phi(d_{obs}) \sim 1$. Clearly, the (unique and stable) selected solution m depends on the choice of the stabilizing term $s(m)$ [14–19]. In this study, three different kinds of $s(m)$ have been tested:

- minimum gradient norm (MGN), $s_{MGN}(m) = \left\|\frac{\Delta \mathrm{m}}{\sigma_m}\right\|_{L2}$;
- minimum gradient L1-norm (MGN-L1), $s_{MGN-L1}(m) = \left\|\frac{\Delta \mathrm{m}}{\sigma_m}\right\|_{L1}$;
- minimum gradient support (MGS), $s_{MGS}(m) = \sum_{k=1}^{M} \frac{\left(\frac{\Delta \mathrm{m}}{\sigma_m}\right)_k^2}{\left(\frac{\Delta \mathrm{m}}{\sigma_m}\right)_k^2 + 1}$, in which, M is the number of model parameters.

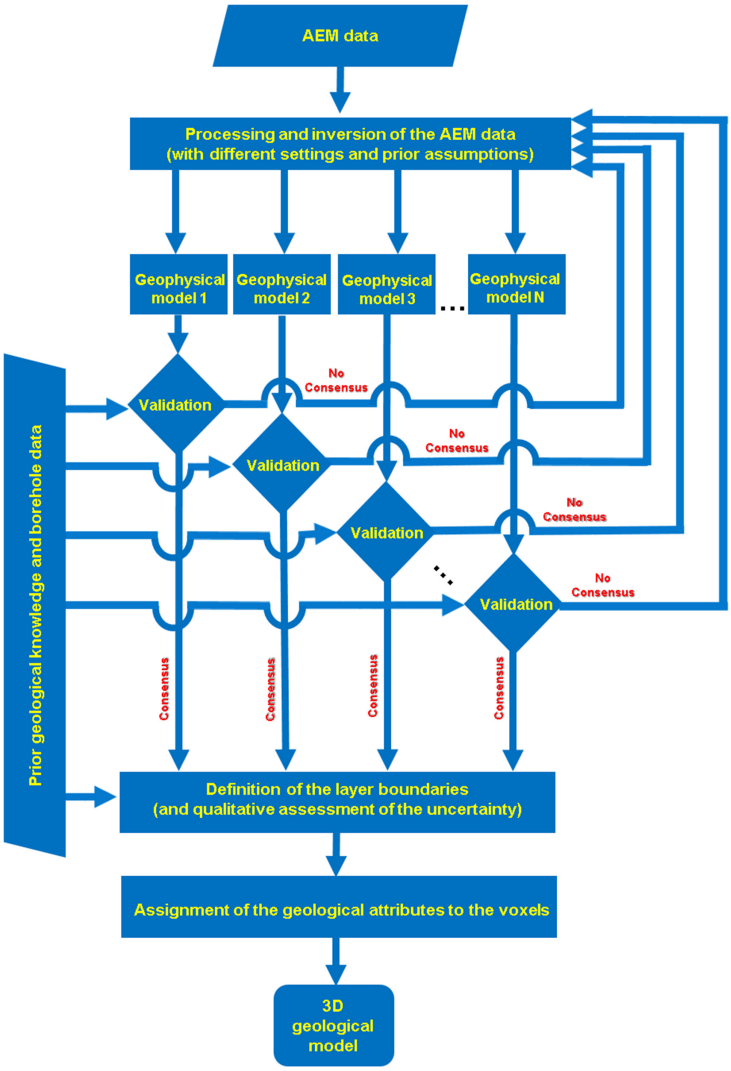

Fig. 4. The flowchart describing the iterative process between geologists and geophysicists aiming at the development of the geomodel integrating all the diverse pieces of knowledge (geophysical, but also prior geological information, wells, etc.) into a coherent picture.

3 The Results

The first, very evident, difference obtained through the new reprocessing and inversion workflow is clear when we compare the original CDIs against the new inversions (see, for example, Fig. 5 and Fig. 6).

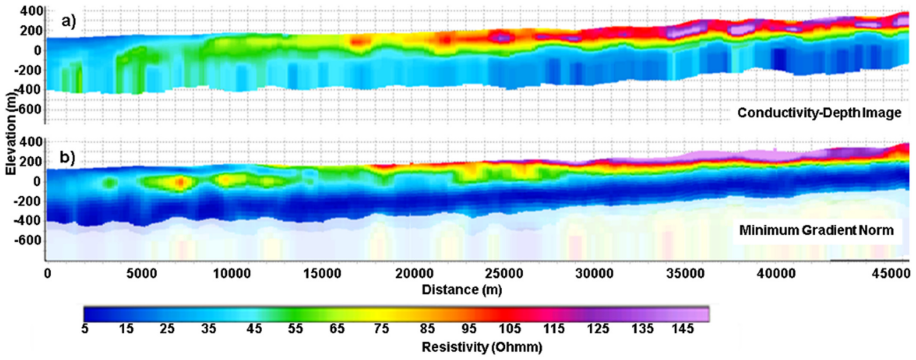

Fig. 5. Comparison between the original CDI (a) and one of the new (Minimum Gradient Norm) results (b).

In particular, as expected, the CDI results are generally characterized by higher lateral variability, since every individual B-field curve is mapped into the associated 1D resistivity model independently, whereas the MGN regularization (as it minimizes, the vertical and lateral variations of the resistivity model) imposes some degree of spatial coherence. Considering, for example, Fig. 5a, as discussed in detail in the recent [20], CDI's lateral heterogeneity is evident not only in the shallow, right, portion of the section, where resistive inclusions are evident, but, also, at depth, along the flight line, where spurious lateral oscillations of the electrical properties are visible. On the other hand, the MGN result in the same figure (Fig. 5b) is laterally more consistent. Despite the lateral coherence of the MGN result, the reconstruction of resistive heterogeneities – at a distance of approximately 10 km, well-separated from the resistive superficial unit by an evident conductive formation (very differently from what is retrieved by the CDI) – is not prevented.

These might appear as minor details, but not when a quantitative geological modelling needs to be performed. This is the case every time a geomodel needs to capture the essential geological features to be included in a subsequent effective hydrogeological simulation. In this respect, it is worth mentioning the interesting resistive features embedded into the conductive surroundings and located between 20 and 30 km: they have been interpreted as possible glacial paleovalleys. The impacts of these possible geological structures are not only interesting in the scientific sense – as their existence would require rediscussing the current regional stratigraphy and support the occurrence of Sturtian glaciation in the West Africa craton (compatible with the Neoproterozoic Snowball Earth hypothesis) – but also from a hydrogeological point of view since they can act as good groundwater reservoirs and they would definitely play a big role as preferential paths for the groundwater modelling.

The MGN-L1 regularization (an example is shown in Fig. 6b) provides results, again, significantly different from the corresponding CDI sections (Fig. 6a), and, at the same time, quite blocky. This is, indeed, not surprising as the L1-norm favors the retrieval of sparse solutions [21].

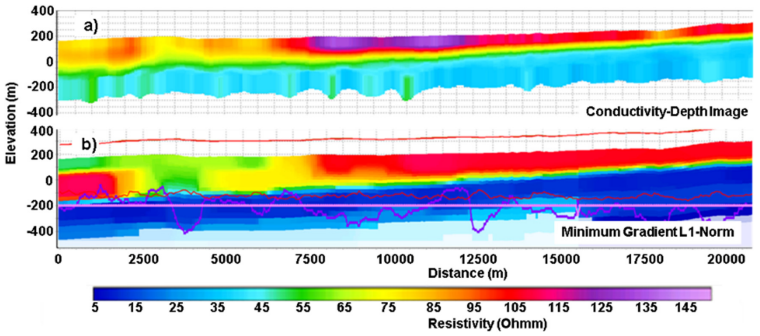

Fig. 6. Comparison between the original CDI (a) and one of the new Minimum Gradient L1-norm results (b).

Similar conclusions can be drawn by using the MGS regularization. In this respect, Fig. 7 shows a comparison between the (more standard) MGN and the MGS solutions [22].

Clearly, during the iterative geophysical-geological interpretation (Fig. 4), only the inversion results characterized by similar levels of data misfits have been considered and compared.

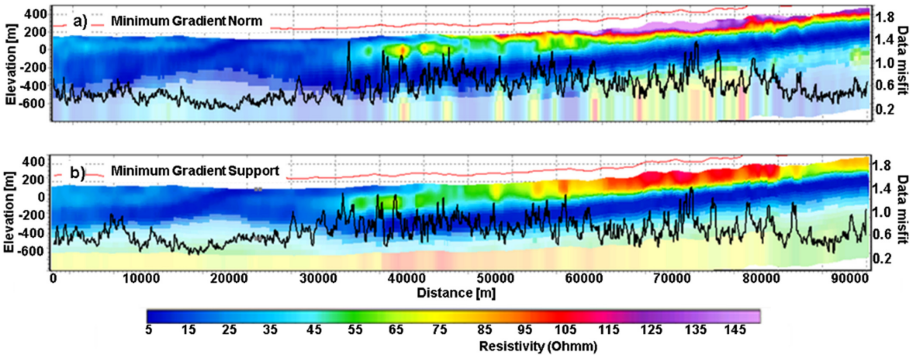

Fig. 7. Comparison between a smooth (MGN) solution (a) and a sharp (MGS) result (b). The black lines show the data misfits.

For example, the solutions in Fig. 7 can be considered equivalent from a purely geophysical point of view (but, definitely, not in their possible geological interpretations) as the misfits between the calculated and observed data (black lines in panels (a) and (b) in Fig. 7) are comparable.

Not only the variability with respect to different regularization strategies, but also the sensitivity with respect to the possible choices of the σ_m values (in particular for the horizontal components of the model variation) when using the same stabilizer had to be tested. In this regard, for example, Fig. 8 and Fig. 9 demonstrate the effects of two

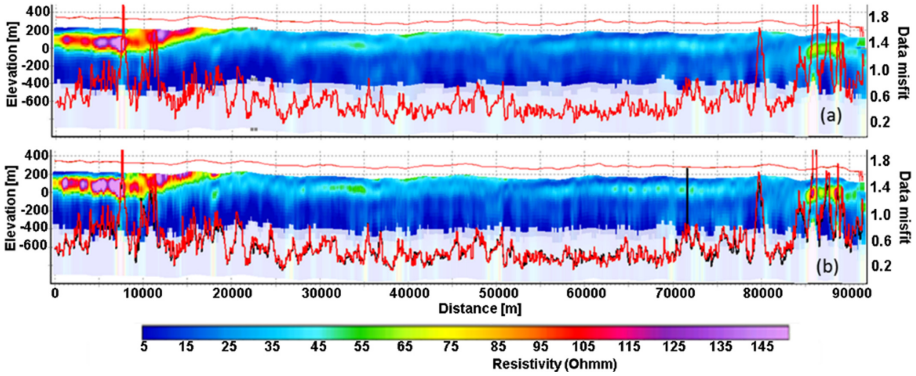

Fig. 8. Comparison between two smooth (MGN) solutions with different lateral constraints: tighter for (a) than for (b). The red line – panel (a) – represents the data misfit for the tighter case (for convenience, it is shown also in panel (b)); the black line is the data misfit for the solution in the panel (b).

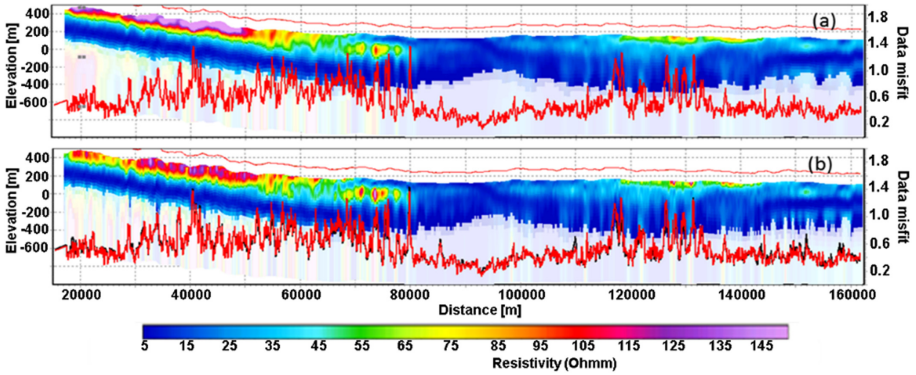

Fig. 9. Comparison between two smooth (MGN) solutions with different lateral constraints: tighter for (a) than for (b). The red line – panel (a) – represents the data misfit for the tighter case (for convenience, it is shown also in panel (b)); the black line is the data misfit for the solution in the panel (b).

different weights for the horizontal constraints. Again, by merely considering the geophysical data, it would not be possible to decide which one is the best as the data misfit associated with the two significantly different models are largely overlapping (black and red lines in Fig. 8b and Fig. 9b).

Concerning all the inversion results, it is worth noting the considerable depth of investigation (indicated as a white mask, for example, in both panels of Fig. 9); generally, the geophysical model parameters could be considered sensitive to the data down to the remarkable depth of $\sim$500 m. This, not only, demonstrates, once more,

the quality of the original data, but, also, confirms that the survey was designed for deep exploration and not for high-resolution shallow investigations. Therefore, the new inversions provide important insights on the geological settings and highlight resistive, relatively shallow structures, possibly relevant as groundwater resources.

4 Conclusions

This research is intended to further elaborate on the recent results discussed in [20]. In [20], Dzikunoo et al. discuss the stratigraphic interpretation of reprocessed airborne electromagnetic data in the Nasia basin in Northern Ghana; here, we show some of the geophysical inversions performed in the sedimentary portion of the White Volta basin that were partially used for the construction of the geomodel of the Nasia basin.

In particular, we show how ill-posed the inversion problem is (considering the finite number of noisy measurements); we demonstrate how solutions, characterized by similar level of compatibility with the observed data, can be significantly different (with potentially large consequences in terms of subsequent geological interpretation). We used that large number of geophysical models for the effective implementation of the flowchart in Fig. 4. Thus, since the different geophysical results are fitting the data equally well, from a mere geophysical perspective, they should be all considered satisfactory. For this reason, the contribution of the geologists (with their "prejudices" about the possible geological structures) is fundamental. From an epistemological point of view, the geophysics has been used to falsify some of the geological alternatives - i.e. those that were not fitting also the geophysical data [23]. In the same line of reasoning, the multiple retrieved geophysical models have been used to assess (at least in a qualitative way) the uncertainty of the inferred structures. Definitely, a more systematic way to investigate the model space could be implemented through stochastic inversion of the data. Unfortunately, this was still found unpractical due to the high computational cost of these kinds of approaches.

This study shows also that, though Conductivity Depth Imaging is an extremely valuable tool for mineral exploration, most likely, for quantitative geological modelling, different approaches (including dedicated processing and inversion strategies) can be beneficial.

Furthermore, the present work demonstrates that the large amounts of geophysical data, originally collected for mineral exploration purposes can be effectively used for (hydro)geological mapping. This might be relevant every time groundwater mapping is a priority, but the large costs of the geophysical data acquisitions prevent any significant initiative.

References

1. Fugro airborne surveys: Airborne geophysical survey of the Volta River Basin and Keta Basin logistics and processing report Geotem areas 1 to 8. Job. N. 06401 (2008)
2. Fugro airborne surveys: Airborne geophysical survey of the Volta River Basin and Keta Basin logistics and processing report Geotem regional survey. Job. N. 06401 (2008)
3. Macnae, J.C., Smith, R., Polzer, B.D., Lamontagne, Y., Klinkert, P.S.: Conductivity-depth imaging of airborne electromagnetic step-response data. Geophysics **56**, 102–114 (1991)
4. Christiansen, A.V., Auken, E., Kirkegaard, C., Schamper, C., Vignoli, G.: An efficient hybrid scheme for fast and accurate inversion of airborne transient electromagnetic data. Explor. Geophys. **47**(4), 323–330 (2016)
5. Smith, R., Annan, P.: The use of B-field measurements in airborne time-domain system: Part I. benefits of B-field versus dB/dt data. Explor. Geophys. **29**, 24–29 (1998)
6. Auken, E., et al.: An overview of a highly versatile forward and stable inverse algorithm for airborne, groundbased and borehole electromagnetic and electric data. Explor. Geophys. **46**(3), 223–235 (2015). https://doi.org/10.1071/eg13097
7. Wilson, G.A., Raiche, A., Sugeng, F.: 2.5D inversion of airborne electromagnetic data. Explor. Geophys. **37**, 363–371 (2006)
8. Cox, L.H., Wilson, G.A., Zhdanov, M.S.: 3D inversion of airborne electromagnetic data using a moving footprint. Explor. Geophys. **41**, 250–259 (2013)
9. Ley-Cooper, A.Y., et al.: Airborne electromagnetic modelling options and their consequences in target definition. Explor. Geophys. **46**, 74–84 (2014). https://doi.org/10.1071/eg14045
10. Auken, E., Christiansen, A.V., Westergaard, J.H., Kirkegaard, C., Foged, N., Viezzoli, A.: An integrated processing scheme for high-resolution airborne electromagnetic surveys, the SkyTEM system. Explor. Geophys. **40**, 184–192 (2009)
11. Vignoli, G., Gervasio, I., Brancatelli, G., Boaga, J., Della Vedova, B., Cassiani, G.: Frequency-dependent multi-offset phase analysis of surface waves: an example of high-resolution characterization of a riparian aquifer. Geophys. Pros. **64**, 102–111 (2015)
12. Viezzoli, A., Munday, T., Auken, E., Christiansen, A.V.: Accurate quasi 3D versus practical full 3D inversion of AEM data – the Bookpurnong case study. Preview **149**, 23–31 (2010). https://doi.org/10.1071/PVv2010n149p23
13. Commer, M., Hordt, A., Helwig, S., Scholl, C.: Threedimensional inversion of time-domain EM data with highly constrained model complexities. In: 20 Kolloquium Elektromagnetische Tiefenforschung, pp. 114–123 (2003)
14. Zhdanov, M.S., Vignoli, G., Ueda, T.: Sharp boundary inversion in crosswell travel-time tomography. J. Geophys. Eng. **3**(2), 122–134 (2006)
15. Ley-Cooper, A.Y., et al.: Airborne electromagnetic modelling options and their consequences in target definition. Explor. Geophys. **46**(1), 74–84 (2015)
16. Vignoli, G., Sapia, V., Menghini, A., Viezzoli, A.: Examples of improved inversion of different airborne electromagnetic datasets via sharp regularization. J. Environ. Eng. Geophys. **22**(1), 51–61 (2017)
17. Pagliara, G., Vignoli, G.: Focusing inversion techniques applied to electrical resistance tomography in an experimental tank. In: XI International Congress of the International Association for Mathematical Geology, Liège, Belgium (2006)
18. Vignoli, G., Zanzi, L.: Focusing inversion technique applied to radar tomographic data. In: Near Surface – 11th European Meeting of Environmental and Engineering Geophysics, European Association of Geoscientists & Engineers, Palermo (2005)

19. Vignoli, G., Deiana, R., Cassiani, G.: Focused inversion of vertical radar profile (VRP) traveltime data. Geophysics **77**(1), H9–H18 (2012)
20. Dzikunoo, E.A., Vignoli, G., Jørgensen, F., Yidana, S.M., Banoeng-Yakubo, B.: New regional stratigraphic insights from a 3D geological model of the Nasia sub-basin, Ghana, developed for hydrogeological purposes and based on reprocessed B-field data originally collected for mineral exploration. Solid Earth **11**, 349–361 (2020)
21. Utsugi, M.: 3-D inversion of magnetic data based on the L1–L2 norm regularization. Earth Planets Space **71**(1), 1–19 (2019). https://doi.org/10.1186/s40623-019-1052-4
22. Vignoli, G., Fiandaca, G., Christiansen, A.V., Kirkegaard, C., Auken, E.: Sharp spatially constrained inversion with applications to transient electromagnetic data. Geophys. Prospect. **63**(1), 243–255 (2015). https://doi.org/10.1111/1365-2478.12185
23. Tarantola, A.: Popper, Bayes and the inverse problem. Nat. Phys. **2**, 492 (2006). https://doi.org/10.1038/nphys375